Diamond based relaxometry for biosensing

Sharmin, Rokshana

DOI:
10.33612/diss.229110585

Chapter 4

Intracellular quantum sensing of free radical generation induced by acetaminophen (APAP) in mitochondria and the nucleus of macrophages

[1]Rokshana Sharmin, [1]Anggrek Citra Nusantara, [1]Linyan Nie, [1]Kaiqi Wu, [1]Arturo Elias Llumbet, [1]Willem Woudstra, [1*]Romana Schirhagl

1. Groningen University, University Medical Center Groningen, Dept. Biomedical Engineering, Antonius Deusinglaan 1, 9713 AV, Groningen, The Netherlands

Submitted to Small

Abstract

Acetaminophen overdoses cause cell injury in the liver. It is widely accepted that liver toxicity is initiated by the reactive APAP metabolite N-acetyl-p-benzoquinone imine (NAPQI), which first depletes glutathione and then irreversibly binds to mitochondrial proteins and nuclear DNA. As a consequence, mitochondrial respiration is inhibited and DNA strands breaks. NAPQI also promote oxidative stress since glutathione is one of the main free radical scavengers in the cell. However, so far it is unknown where exactly free radicals are generated. In this study, we used relaxometry, a novel technique that allows nanoscale MRI detection of free radicals. The method is based on fluorescent nanodiamonds (FNDs), which change their optical properties based on their magnetic surrounding. To achieve subcellular resolution, these nanodiamonds were targeted to cellular locations, *i.e.* the cytoplasm, mitochondria, and the nucleus. Since relaxometry is sensitive to spin noise from radicals we were able to measure the radical load in these different organelles. For the first time, we measured APAP-induced free radical production in an organelle-specific manner, which helps to predict and better understand cellular toxicity.

Introduction

Acetaminophen is the most used analgesic and antipyretic drug. Overdose of APAP can lead to acute liver poisoning and death [1,2]. Physiologically, APAP is metabolized in the liver, by cytochrome P450s [3-5], which produces the active metabolite N-acetyl-P-benzoquinone imine (NAPQI) that

is efficiently detoxified by conjugation with glutathione [6,7]. However, higher doses of APAP (0.5 to 10mM/mL) lead to critical depletion of glutathione, formation of NAPQI adducts with mitochondrial proteins, and oxidative stress. This oxidative stress amplifies the formation of reactive oxygen species (ROS) and reactive nitrogen species (RNS), causing mitochondrial membrane permeability transition, pore opening and cessation of adenosine triphosphate (ATP) synthesis. In addition, mitochondrial matrix swelling ruptures the outer membrane and releases endonucleases, which cause nuclear deoxyribonucleic acid (DNA) fragmentation. Together, the nuclear DNA damage and the extensive mitochondrial dysfunction result in necrotic cell death [8].

There are many methods to detect cellular toxicity, including imaging, cell loss, monitoring of DNA damage, measurement of the reduction of glutathione levels, and detection of intracellular ROS and mitochondrial membrane potential [9]. The intracellular concentration of reactive species is one of the most important indicators of liver toxicity. However, most methods do not differentiate between the different types of reactive species. Among ROS, free radicals such as hydroxyl radical, nitric oxide or superoxide are the most difficult to measure due to their low abundance and reactivity [10]. Free radicals are responsible for cellular damage by reacting with cellular components such as proteins, lipids, and DNA [11]. Therefore, it is very important to carry out reliable measurements of the concentration or relative levels of free radicals in addition to the conventional measurements of ROS. Several methods are available for free radical detection. Chromatographic methods are used for the separation and identification of adducts or reaction products that free radicals produce with other molecules. Spectrophotometric methods are based on the reaction between radicals and redox substances; the resulting differences in absorbance at different wavelengths gives semi-quantitative data of free radical levels [12]. However, these methods do not offer any spatial resolution.

Fluorescent and chemiluminescent probes and electron spin resonance (ESR/EPR) offer at least some spatial resolution, but these techniques do not allow subcellular resolution due to the diffusion of dye molecules [12]. For example, 2'-7'dichlorofluorescin diacetate (DCFH-DA) is a probe generally used for the direct measurement of intracellular reactive oxygen species including all kinds of radicals and non-radical species [13,14]. However,

because non-radical species are in a much higher in concentration than radicals, these are the main components contributing to the detected signal.

Quantum sensing is an appealing option to solve the spatial limitations of the aforementioned methods since it can detect free radicals at a nanomolar range with nanoscale resolution. The method requires the use of fluorescent nanodiamonds (FNDs). These are promising nanoprobes, for their stable fluorescence and excellent biocompatibility [15]. They have unique magneto-optical properties and can be used as probes for magnetic resonances [16,17]as well as pressure [18-20] and temperature measurements [21]. Due to their unprecedented sensitivity, FNDs can detect even the faint magnetic resonance of a single electron or even a few nuclear spins [22]. Since these signals are strongly distance dependent, FNDs only sense their immediate surrounding up to a few nanometers. As a result, the diamond probes have to be close to the molecules that need to be detected. Our group already proved that FNDs can be used to detect free radicals in living cells [23,24]. Since their free electrons cause spin noise, they can be detected with relaxometry measurements (also called T1 measurements). This is a specific mode of diamond magnetometry that is purely optical and does not require microwaves [25]. With this method, radicals can be detected with nanoscale resolution in nanomolar concentrations.

In this study, our aim was to predict APAP-induced cellular toxicity at an early stage before cell death by measuring free radical concentrations. For the first time, we achieved spatial resolution, which allowed differentiating between radical generation in the cytosol, the mitochondria, and the nucleus. To achieve this goal, we used diamond-based quantum sensing and compared with conventional methods.

Materials and Methods

Cell experiments:

Macrophage J774A.1 cells were grown in high glucose DMEM containing 10% (v/v) FBS. This medium was supplemented with 1% streptomycin and 1% penicillin. Cells were grown in T-75 cell culture flasks containing (0.5–1) $\times 10^6$ cells/mL and kept in a humidified atmosphere containing 5% CO_2 at 37°C. On the following day, when the number of cells reached 5×10^6 cells/mL, cells were removed from the T-75 flask and seeded in a four quarters glass bottom Petri dish (Greiner Bio-One, Germany) at 30,000

cells/cm^2 with 500 μL DMEM medium and kept in the incubator at 37°C in the presence of 5% CO_2.

The FND incubation process in macrophage cells was described in our previous paper [15]. For measurements in cells, 1 μg/ml suspensions of bare FNDs, FNDs targeted to mitochondria (MIT-FNDs) and to the nucleus (NLS-FNDs) were prepared with high glucose DMEM medium for targeting cytoplasm, mitochondria, and nucleus respectively. Then cells were treated with different concentrations of APAP varying the incubation time.

In the case of 18 h treatment we incubated different targeting nanoparticles 2 h before the treatment. In the 3, 6 and 9 h groups, different targeting FNDs were incubated overnight without treatment. Next morning, we added differently concentrated APAP solutions with different concentrations to the DMEM medium. Then relaxometry assays were performed to determine the different stress responses. After that, cells were fixed with 4% formaldehyde and washed with phosphate buffer saline before staining with 4′,6-diamidino-2-phenylindole (DAPI) and Fluorescein (FITC)-Phalloidin as previously described [26] to visualize nuclei and F-actin, respectively.

Preparation of FNDs:
To determine the T1 relaxation time, we used 70 nm FNDs (Adamas Nanotechnologies, NC, USA). These FNDs are produced by high-pressure high-temperature (HPHT) synthesis followed by irradiation and high temperature annealing. This process leads to bright particles containing about 300 nitrogen vacancy (NV^-) centers per particles (determined by the manufacturer). As a last step of production, FNDs are cleaned with oxidizing acids. As a result, they are oxygen terminated. These particles are widely used for different applications and have been characterized in the literature [27-29]. In this article we used three types of particles, which are shown in Fig 1(a): bare

FNDs for measurements in the cytoplasm, particles for mitochondrial targeting (MIT-FND) and particles for nucleus targeting (NLS-FND).

FNDs for cytoplasmic measurements: For cytoplasmic measurements, a suspension of bare FNDs 1 μg/mL was prepared in high glucose DMEM medium. Then the solution was added to the cells. The solution containing

FNDs remained in the dish until the end of the experiment. We have shown earlier that FNDs escape from the endosomes under these conditions [24]. To further confirm the location of the particles, we performed a Calcein assay (see supplementary information Fig S5). The Calcein assay is widely used to evaluate the presence of particles inside the cytoplasm. Calcein is a cell membrane impermeant fluorescent dye and emits green light in endosomes and lysosomes. If particles escape the endosome, they do not colocalized with green vesicles. The assay was performed in the presence of different concentrations of APAP and we added 0.25 mM calcein with 1 μg/mL FNDs. After 2 h of FNDs and calcein incubation, we added APAP for about 18 h. At the end of the treatment, the cells were washed with PBS 3 times and fixed with 4% formaldehyde before taking confocal images. The colocalization of FNDs with the vesicles was quantified with the Manders' coefficient using the Fiji plugin "JACop"[30,31]. The Manders' coefficient is used to quantify the degree of colocalization between fluorophores. Its range is between 0 to 1. Larger coefficient means stronger evidence of co-localization between fluorophores with the target organelles [32,33].

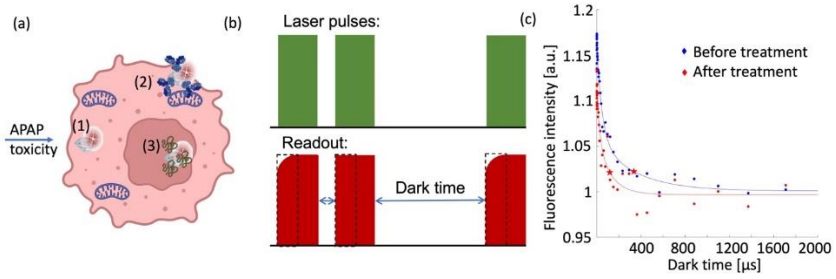

Figure1: Experiments conducted in this paper. (a) schematic representation of the conducted experiments. 3 different particles were used for sensing free radical generation in macrophage J774A.1 cells. (1) bare fluorescent nanodiamonds (FNDs), which allow measurements in the cytosol, (2) FNDs coated with an antibody targeting the mitochondrial surface (MIT-FNDs), and (3) FNDs coated with a nuclear localization signal (NLS-FNDs) (b) schematic representation of the relaxometry sequence which is used to measure the spin noise from free radicals. The laser pulses pump the NV centers in the bright ms=0 state of the ground state. After different dark times another laser pulse probes if the NV centers are still in the bright state or have returned to the darker equilibrium. The dotted rectangles indicate the read window. (c) An

example of 2 representative T1 curves measured in macrophage J774A.1 cells before and after they were challenged with APAP for 18 h. Red stars indicate the T1 time.

FNDs for mitochondrial measurements: Anti-VDAC2 antibody (GTX104745, GeneTex, The Netherlands)) coated the FNDs were targeted to the surface of mitochondria. To prepare these particles, anti VDAC2-antibodies were diluted to a concentration of 0.089 mg/ml (1:100 dilution, as suggested by the manufacturer). The antibodies were mixed with FNDs (1 μg/ml) in a 1:2 ratio for 1 to 2 min while vortexing. This was followed by incubation at room temperature for 15 min to allow antibodies to adsorb on the FNDs. We have shown before that these nanodiamonds can be targeted to the mitochondria in macrophages [24]. Malvern instruments (Dynamic light Scattering, Malvern instruments ltd, Malvern, UK) were used to evaluate size changes after the modification of nanodiamonds to exclude aggregates of the coated FNDs (1 μg/mL) in medium (see supplementary information Fig S1).

FNDs for nuclear measurements: For attaching NLS to the FNDs, we used 1-ethyl-3-(3-dimethylaminopropyl)-carbodiimide hydrochloride (EDC, Merck, The Netherlands) and N-hydroxysuccinimide (NHS, Merck, The Netherlands). The resulting surface groups were reacted with amine groups of SV40 T-Ag-derived NLS peptide (PKKKRKVEDPYC) (AnaSpec-AS63788) to form carbamide. Specifically, 0.5 mL freshly prepared EDC/NHS (30/15 $\mu g \cdot mL^{-1}$, respectively) solution made with cold ultrapure water was added to 200 μg FND in 1 mL ultrapure water. The reaction was stirred for 1 h in ice to activate the carboxyl groups on the nanodiamond surface. Then 50 μg NLS peptide in 0.5 mL ultrapure water was added to the activated FND solution. The reaction was performed overnight at room temperature. Unconjugated NLS peptides and the residues of EDC/NHS were removed by dialysis against (Spectra/Pore, MWCO 10,000-16,000) demi water. After purification, NLS modified FND (NLS-FND) was concentrated by PEG (MW: 8,000 Da, Merck, The Netherlands) and sterilized using sonication. NLS-FNDs were sonicated 10 to 15 min before mixing with high glucose DMEM cell culture medium. A Malvern Zetasizer nanosystem (Dynamic light Scattering, Malvern instruments ltd, Malvern, UK) was used to evaluate size changes after the modification of nanodiamonds to exclude severe aggregation of the coated FNDs (1 μg/mL) in medium (see supplementary information Fig S1).

To confirm that NLS-FNDs colocalizes with the nucleus, we used Manders' coefficients as described above.

Evaluation of spin sensing capacity of antibody coated and NLS conjugated FNDs:

To evaluate the spin sensing capacity of bare-FNDs, MIT-FNDs and NLS-FNDs, we measured T1 relaxation times of these particles in the presence of different concentrations of $GdCl_3$ solution in DMEM medium. Gadolinium has a strong signal and is thus used as a contrast agent in MRI. For all particles we were able to confirm that they respond to spin noise by lowering T1 as expected. Before performing the experiment, we instantly prepared different Gadolinium stock solutions (1, 10, 100, and 1000 μM) by dissolving gadolinium (III) chloride (439770-5G, Sigma-Aldrich, Germany) in MQ water. During the experiments, we added 5 μL from each stock solution to generate the desired 0.01, 0.1, 1, and 10 μM working concentrations.
On the other hand, we coated Petri dishes with bare-FNDs, MIT-FNDs and NLS-FNDs inside the flow hood. There, 1 μL of bare FNDs, MIT-FNDs or NLS-FNDs (1 μg/ml) suspension were spread on different glass bottom Petri dishes and continuously spreading with tips to avoid aggregation while drying. Then the Petri dish was focused on the confocal plane of a home built confocal microscope[34]. We scanned the Petri dish to select single FND and added 500 μL DMEM medium and measured T1. Subsequently, we added 0.01, 0.1, 1 and 10 μM $GdCl_3$ solution and measured T1 (see supplementary information Fig S2).

Relaxometry:

After completion of the desired time of drug treatment with APAP, the Petri dish was focused at the focal point of a home-built magnetometry setup that has been explained previously [35]. In short, the setup is a confocal microscope with the capability to perform the required pulsing sequences (shown in Fig 1 (b)). To perform the T1 measurement, a single FND inside the cell (confirmed by confocal imaging) was selected. We chose particles with a count rate between 1×10^6 and 3×10^6 photon counts per second. Particles with larger count rates are usually large aggregates while smaller count rates indicate a small particle. Such small particles move faster and emit

less photons per time unit and thus deliver less reproducible data. During a relaxation time measurement, the NV centers are first initialized into the bright ms=0 state of the ground state by a laser pulse (5 μs). Then we probed after varying dark times if they are still in this state or if they have returned into the darker equilibrium between the ms=0 and ms=+1 or -1 states. This is done by counting photons in the first 0.490 μs of the pulse (see Fig 1(b)). Lower photon counts indicate that the NV centers have already returned to the equilibrium. The time it takes the NV centers to relax into the equilibrium, the T1 time, decreases in presence of spin noise. T1 is equivalent to T1 in conventional magnetic resonance imaging (MRI). However, since FNDs interact only with spins within a few nm, this method offers nanoscale resolution. Since contributing nuclear spins such as hydrogens are constant throughout the experiment and three orders of magnitude smaller, T1 gives a quantitative measure to assess radical generation in the particles surrounding. While an individual T1 measurement takes on the order of microseconds, we repeated the pulse train for 10000 times to improve the signal to noise ratio. The entire experiment lasts around 10 min, and each experiment was repeated 3 times independently.

DCFH-DA assay:

Intracellular ROS were measured using the cell permeable probe 2′, 7′ – dichlorodihydro fluorescein diacetate (DCFH-DA), which measures the total intracellular ROS that was produced between adding the compound and detection. After entering the cell, DCFH-DA was deacetylated and later oxidized by ROS to 2′, 7′ – dichlorodihydro fluorescein (DCF) which is fluorescent. After APAP treatment, cells were incubated with 0.2 μg/mL of a 5 μM DCFH-DA solution for 30 min at 37°C. Subsequently cells were washed with phosphate buffered saline (PBS), and we immediately acquired 2D confocal images with a Zeiss 780 confocal microscope (Zeiss, Sliedrecht, The Netherlands), using excitation and emission wavelengths of 485 and 582 nm, respectively. The mean fluorescence intensity was measured using the Fiji software. Each experiment was repeated 3 times, and the number of cells per experiment was more than 50.

DHE assay:

Dihydroethidium (DHE) itself displays blue fluorescence in the cell cytoplasm. However, the oxidized form 2-hydroxyethidium intercalates into DNA and exhibits red fluorescence. Dihydroethidium DHE (abcam) was used to determine the intracellular superoxide radical levels qualitatively [36]. DHE enters the cells and is oxidized to ethidium, which binds to DNA to produce red fluorescence. In this study, a DHE solution (2 µg/mL) was prepared in DMEM medium and added to macrophage cells immediately after completing the APAP treatment. Then the cells were incubated for 10 min at 37°C and 5% CO_2 in the incubator. Subsequently cells were washed with ice-cold DMEM medium and 2D Confocal images were taken with a Zeiss 780 confocal microscope (Zeiss, Sliedrecht, The Netherlands). DHE excitation and emission wavelengths are 514 and 580 nm, respectively. The mean fluorescence intensity was quantified using FIJI software. Each experiment was repeated 3 times, and the number of cells per experiment was more than 50.

MTT assay:

The MTT assay is used to measure cellular metabolic activity as an indicator of cell viability, proliferation, and cytotoxicity. This colorimetric assay is based on the reduction of a yellow tetrazolium salt (3-(4,5-dimethylthiazol-2-yl)-2,5-diphenyltetrazolium bromide or MTT, Sigma Aldrich, Zwijndrecht, the Netherlands) to purple formazan crystals by metabolically active cells. Viable cells contain NAD(P)H-dependent oxidoreductase enzymes that reduce the MTT to formazan. The insoluble formazan crystals are dissolved using a solubilization solution. The resulting, colored solution is quantified by measuring absorbance at 570-650 nanometers using a multi-well spectrophotometer. The darker the solution, the higher the number of viable, metabolically active cells. To test the viability of cells after APAP treatment, cells were treated with 0.05% MTT and serum free medium for two hours. After two hours of incubation, the cells were washed with PBS. Subsequently, formazan crystals were dissolved using 2-propanol and the absorption of the purple solution was measured using a Synergy HT microplate reader, Biospx, USA at 570 to 650nm. In this viability assay 80 – 120% absorption of the control is the normal range [37].

Statistical analysis:

Statistical analysis of all data was conducted by using GraphPad Prism version 6. Significance was tested by using a two-way ANOVA followed by a Tukey post hoc test. All statistical tests were compared to the control group and defined as: ns $p>0.05$, $^{*}P \leq 0.05$, $^{**}P \leq 0.01$, $^{***}P \leq 0.001$, $^{****}P \leq 0.0001$.

Results and Discussion

Confirming the subcellular location of diamonds

For bare FNDs it has been shown that they escape from the endosomes and reside in the cytosol after entering the cell [38,39]. There are substantial differences in endosomal escape between cell types [40]. Endosomal escape has also been shown for macrophage J774A.1 cells in the supplementary Fig S5. Although both antibody targeting as well as targeting with NLS are established for other particles, it is important to confirm their subcellular location. For mitochondrial targeting with MIT-FND, this has been confirmed for this cell type by [24].

To confirm that NLS-FND is indeed targeted to the nucleus, we stained the nuclei and determined colocalization between NLS-FND and the nucleus. As a control, we also performed these experiments with bare FNDs (see Fig. 2). There are also some particles that are localized at the nuclear surface in the FND group. This has also been observed in other cell types where FNDs tend to accumulate near the nuclear surface [41]. Almost all particles in the NLS-FND group colocalize with the nucleus, allowing measurements on the nuclear surface.

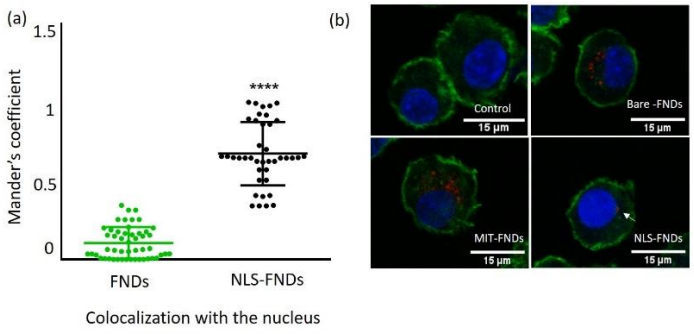

Figure 2: Colocalization of NLS-FNDs with the nucleus. (a) Shows the Manders' colocalization coefficient of NLS-FNDs with the nucleus compared to FNDs. The scatter dot plot shows the standard deviations (unpaired t-test, ****$p \leq 0.0001$). Experiments were repeated 3 independent times. (b) Confocal images of internalized FNDs, MIT-FNDs and NLS-FNDs. (blue: nuclei stained with DAPI, red: FND (with or without coatings, green: FITC-Phalloidin staining the actin filaments).

Detection of APAP-induced intracellular free radical generation

Radical generation in the cytosol: Relaxometry was used to detect APAP induced free radical generation in the cytosol, mitochondria, and the nucleus. After FND incubation, we took confocal images to confirm that FNDs were inside the cell and conducted relaxometry measurement. We treated cells with 3 different doses 0.5 mM, 2 mM and 4 mM of APAP for 3 h, 6 h, 9 h and 18 h and measured free radical generation via relaxometry. Decreasing T1 values indicate that the free radical concentration increased, while increasing T1 indicates a decreasing free radical load [42]. Fig. 3 (a) shows the free radical generation in the cytosol. We found that there are no significant changes in the free radical load in the cytosol in the first hours. Only at the highest concentrations of APAP and the longest incubation (18 h, 2 mM and 4 mM APAP) we observed an increase in radical formation. This radical formation is likely induced by cell death which occurs under these conditions. Cell death under these conditions was confirmed by an MTT assay and confocal images showing reduced cell confluency (see supplementary Fig S4 and S6).

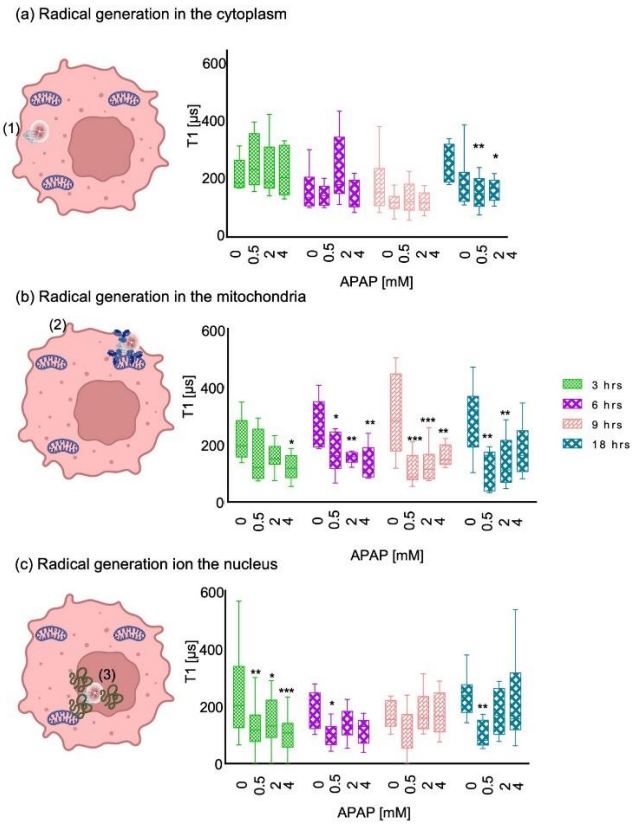

Figure 3: APAP induced free radical response measured by relaxometry. (a) shows the T1 relaxation in cells treated with different concentrations 0.5, 2, 4 mM of APAP and different time points 3, 6, 9, 18 hours measured in the cytosol with FNDs. (b) shows measurements on the mitochondrial surface using MIT-FNDs and (c) shows measurements on the nuclear surface using NLS-FNDs under the same conditions. The data is shown by separated box and whisker plots with minimum and maximum values. Each experiment was repeated 3 independent times. Data were analyzed using two-way ANOVA followed by Tukey post hoc test. Statistical significance is indicated by *P ≤0.05, **P ≤ 0.01, ***P≤0.001.

Radical formation in the mitochondria: In contrast to the cytosol, in mitochondria free radical generation already occurred after 3 h of APAP administration (see Fig 3 (b)) with the highest concentration of APAP (4 mM) and leads to a significant increase in radical formation. At timepoints 6, 9 and 18 h, however, we observed an increase in radical formation for all the concentrations, with the exception of the 18 h 4 mM condition. This finding agrees with the literature. Thekra Al-Belooshi et al. demonstrated that APAP-

induced cellular toxicity in macrophages [43]. They found increased ROS production in cells that were treated with APAP for 18 h compared to a control and compared with the 2 h of treatment. They speculated that this is due to mitochondrial oxidative stress induced by NAPQI adduct formation. Compared to Thekra Al-Belooshi et al., we were able to see changes earlier changes in the stress response earlier which might be related to free radicals being the first response to the adducts, higher sensitivity of our technique or mitochondria being the main source of the response and the earliest responder organelle. At the earlier time points we also observe a clear concentration dependency. In general, the higher the APAP concentration we used, the more pronounced free radical response we observed.

Detection of APAP induced free radical generation in the nucleus: Finally, we also investigated free radical generation on the nuclear surface. The results are shown in Fig. 3 (c). In contrast to the cytosol or mitochondria, we observed free radical generation in the nucleus already at the 3 h timepoint with 0.5, 2, and 4 mM APAP, which represents a fast (3h) and more sensitive (0.5 mM APAP) response when comparing with the other two evaluated compartments. This might explain findings in the literature where relatively low concentrations of APAP (0.1 mM) inhibited DNA synthesis within minutes in V79 Chinese hamster cells. RNA and protein synthesis in V79 cells are inhibited only after longer exposure (3 h) and considerably higher concentrations of APAP (3-10 mM) [44].
Furthermore, DNA strand breaks have been observed, and APAP inhibits both replicative DNA synthesis and DNA repair synthesis in vitro and in animal experimental [45]. While it has been assumed that these DNA alterations are caused by reactive species, we show here that radical species are indeed produced in or close to the nucleus. This finding is supported by reports on EPR spin trapping which has been employed to detect radical production in isolated rat liver nuclei on exposure [46]. However, such studies required the use of spin traps and thus do not allow real time measurements. Besides, those measurements were performed on large ensembles of cells rather than single cells.
Finally, our data shows that radical formation also occurs in the nucleus or that radicals in significant amounts are accumulated there.

Controls without cells: As a control we also performed T1 measurements of the different FNDs exposed to different doses of APAP without cells. In the

absence of cells and their stress response, we did not observe any significant differences from APAP alone (Supplementary Fig S3).

Comparing free radical generation with conventional methods

Cell viability: The metabolic activity of cells was tested with an MTT assay to evaluate the effect of different concentrations of APAP as well as FNDs, MIT-FNDs and NLS-FNDs. During this assay, MTT is converted to the purple formazan by mitochondrial reductase. Only metabolically active cells can convert MTT to formazan. It is important to note that the viability is generally considered equal to the control or if it is between 0.8 and 1.2 values. The results of the MTT assay are shown in the supplementary Fig S4. The cell viability after APAP treatment for 3 h, 6 h and 9 h remain unchanged for all the tested concentrations. For the groups that were treated 18 h with APAP, we observed a reduction in viability in all groups exposed to different concentrations. These findings were consistent for groups containing bare FNDs, MIT-FNDs, and NLS-FNDs, which could be related to the accumulation of free radicals or other reactive oxygen species after long term exposure to APAP. While nano diamonds have been shown to be excellently biocompatible in many different cell types or *in vivo*, it is important to confirm this for every new cell type and every new modification of particles [38,47]. Thus, we included control groups where cells were only treated with bare FNDs, MIT-FNDs, or NLS-FNDs. As expected, none of these groups showed any reduction in cell viability.

Detection of ROS generation by a DCFH-DA assay: ROS production was tested by a DCFDA assay. Using DCFDA as a fluorescent probe, we observed only significant increases in ROS production at the highest dose of APAP (4 mM, Fig. 4(a)). This increase was evident for all time points. When exposed to the lower concentrations, the cells did not increase ROS production significantly.

The results from this method represents the average of a population of cells and the entire intracellular area [48]. More precisely, it detects ROS including all kinds of free radicals and nonradical species such as for instance hydrogen peroxide, superoxide anions or singlet oxygen species [49]. Using DCFH-DA, we observed a high variability between the different cell groups (shown in Fig. 4(b)), which highlights the need for single-cell assays. Also evident

from Fig. 4(b) is that there is no subcellular resolution. The reason is that DCF diffuses freely inside the cells [50]. This is different in T1 measurements, where free radical measurements can be performed at a specific location inside one single cell. Another difference with T1 measurements is that DCFH-DA assays reveal the history of a group of cells rather than the free radical concentration at a specific moment. It is also evident from Figure 4 (a) that the DCFH-DA assay is less sensitive than our T1 measurements even though it measures a much larger sample. The reason might be that it does not allow local detection.

Measuring superoxide by the DHE assay: DHE freely permeates cell membranes and is used extensively to monitor superoxide production [51] DHE is perhaps the most specific and least problematic dye. It detects essentially superoxide radicals, is retained well by cells, and may even tolerate mild fixation [52]. T1 relaxation time in mitochondria and the nucleus were evaluated with the DHE assay. Using the DHE assay, we detected superoxide formation after challenging the cells with 4, 2 and 0.5 mM APAP. As shown in Fig. 4 (c), in almost all the groups we observed an increase in superoxide formation.

Nuclear area: Another way to assess toxicity is to monitor morphological changes. Due to the pronounced effect of APAP on the nucleus we observed the changes in nuclear area. The results are shown in Fig 4 (c). At 3, 6 and 9 hours, we did not observe any significant morphological changes. At the 18 h timepoint where we observed cell death for all the APAP concentrations, the nuclear area is also significantly reduced.

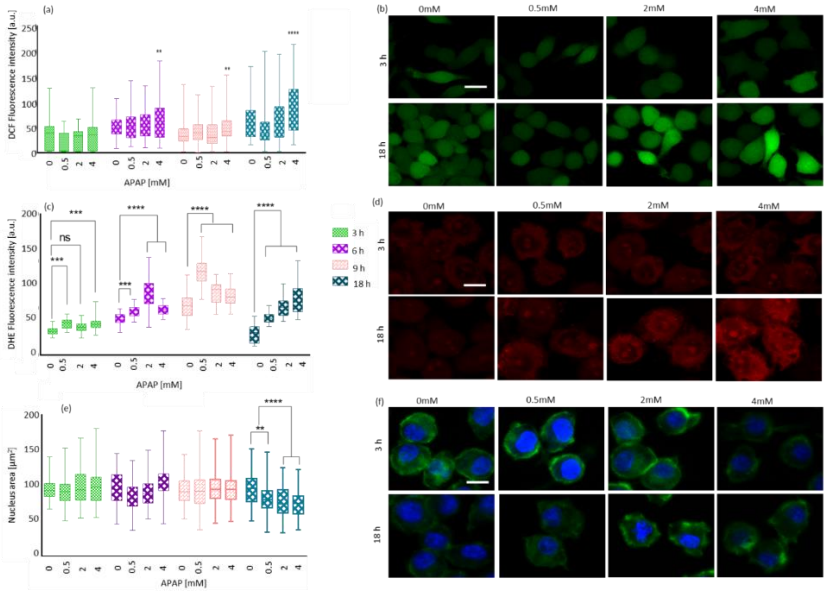

Figure 4: APAP induced ROS generation and total nuclear area on timepoints 3, 6, 9 and 18 h treated with 0, 0.5, 2 and 4 mM APAP. (a) The DCFH-DA assay shows intracellular ROS generation after different time points of APAP treatment. (b) representative confocal images from the DCF stained macrophage J774A.1 cells. (c) Superoxide radical formation measured by the DHE (Dihydro ethidium) assay (d) Confocal images shows the fluorescence intensity inside the cell caused by superoxide determined by the DHE assay. (e) Total nuclear area. (f) Confocal images showing the reduction in total nucleus area after APAP treatment compared to the control group. Here nuclei were stained with DAPI shown in blue and actin fibers were stained with phalloidin-FITC shown in green. Scale bars are 15µm. The data is shown by separated box and whisker plots with minimum and maximum values. Each experiment was repeated 3 independent times. Data were analyzed using two-way ANOVA followed by a Tukey post hoc test. Statistical significance is indicated by *P ≤0.05, **P ≤ 0.01, ****P≤0.0001.

Conclusion

We demonstrated the detection of radical generation with subcellular resolution in living macrophage J774A.1 cells. More specifically, we were able to show how cells respond to being challenged with APAP and where exactly the radical formation occurs. We found that while there is a relatively low radical load in the cytosol, there is an increase in radical formation in the mitochondria and the nuclear surface. Our measurements were able to detect

the changes in radical load early and in sub-lethal doses Compared to conventional methods, relaxometry allows to detect radicals specifically rather than all kinds of ROS. Furthermore, our technique allows monitoring the current state of the cells while the conventional methods reveal the history of the sample. Our findings confirm the broadly accepted theory that the stress responses to APAP in macrophages happen primarily in the mitochondria and to some extend in the nucleus. While these findings are not surprising, the relaxometry method gives us a tool to directly measure the radical formation and determine the radical load in specific organelles, which highlights its potential for cellular toxicity evaluation in drug screenings.

References:

1. Litovitz TL, Klein-Schwartz W, Rodgers GC Jr, Cobaugh DJ, Youniss J, Omslaer JC, May ME, Woolf AD, Benson BE. 2001 Annual report of the American Association of Poison Control Centers Toxic Exposure Surveillance System. Am J Emerg Med. 2002 Sep;20(5):391-452. doi: 10.1053/ajem.2002.34955. PMID: 12216043.

2. Lazerow SK, Abdi MS, Lewis JH. Drug-induced liver disease 2004. Curr Opin Gastroenterol. 2005 May;21(3):283-92. doi: 10.1097/01.mog.0000160043.10804.60. PMID: 15818148.

3. Chen W, Koenigs LL, Thompson SJ, Peter RM, Rettie AE, Trager WF, Nelson SD. Oxidation of acetaminophen to its toxic quinone imine and nontoxic catechol metabolites by baculovirus-expressed and purified human cytochromes P450 2E1 and 2A6. Chem Res Toxicol. 1998 Apr;11(4):295-301. doi: 10.1021/tx9701687. PMID: 9548799.

4. Patten CJ, Thomas PE, Guy RL, Lee M, Gonzalez FJ, Guengerich FP, Yang CS. Cytochrome P450 enzymes involved in acetaminophen activation by rat and human liver microsomes and their kinetics. Chem Res Toxicol. 1993 Jul-Aug;6(4):511-8. doi: 10.1021/tx00034a019. PMID: 8374050.

5. Nelson SD. Molecular mechanisms of the hepatotoxicity caused by acetaminophen. Semin Liver Dis. 1990 Nov;10(4):267-78. doi: 10.1055/s-2008-1040482. PMID: 2281334.

6. Hinson JA, Reid AB, McCullough SS, James LP. Acetaminophen-induced hepatotoxicity: role of metabolic activation, reactive oxygen/nitrogen species, and mitochondrial permeability transition. Drug Metab Rev. 2004 Oct;36(3-4):805-22. doi: 10.1081/dmr-200033494. PMID: 15554248.

7. Reid AB, Kurten RC, McCullough SS, Brock RW, Hinson JA. Mechanisms of acetaminophen-induced hepatotoxicity: role of oxidative stress and mitochondrial permeability transition in freshly isolated mouse hepatocytes. J Pharmacol Exp Ther. 2005 Feb;312(2):509-16. doi: 10.1124/jpet.104.075945. Epub 2004 Oct 1. PMID: 15466245.

8. Jaeschke H, Duan L, Nguyen N, Ramachandran A. Mitochondrial Damage and Biogenesis in Acetaminophen-induced Liver Injury. Liver Res. 2019 Dec;3(3-4):150-156. doi: 10.1016/j.livres.2019.10.002. Epub 2019 Nov 1. PMID: 32655976; PMCID: PMC7351365.

9. Jinghai J Xu, Peter V Henstock, Margaret C Dunn, Arthur R Smith, Jeffrey R Chabot, David de Graaf. Cellular imaging predictions of clinical drug-induced liver injury. Toxicol Sci. 2008 Sep; 105(1): 97-105. doi:10.1093/toxsci/kfn109. PMID: 18524759.

10. Lushchak VI. Free radicals, reactive oxygen species, oxidative stress and its classification. Chem Biol Interact. 2014 Dec 5;224:164-75. doi: 10.1016/j.cbi.2014.10.016. Epub 2014 Oct 28. PMID: 25452175.

11. Young IS, Woodside JV. Antioxidants in health and disease. J Clin Pathol. 2001 Mar;54(3):176-86. doi: 10.1136/jcp.54.3.176. PMID: 11253127; PMCID: PMC1731363.

12. Zhang Y, Dai M, Yuan Z. Methods for the detection of reactive oxygen Species. Anal. Methods. 2018; 10: 4625–4638. doi: 10.1039/c8ay01339j.

13. Rao KM, Padmanabhan J, Kilby DL, Cohen HJ, Currie MS, Weinberg JB. Flow cytometric analysis of nitric oxide production in human neutrophils using dichlorofluorescein diacetate in the presence of a calmodulin inhibitor. J Leukoc Biol. 1992 May; 51(5): 496-500.doi:10.1002/jlb.51.5.496. PMID: 1602242.

14. Possel H, Noack H, Augustin W, Keilhoff G, Wolf G. 2,7-Dihydrodichlorofluorescein diacetate as a fluorescent marker for peroxynitrite formation. FEBS Lett. 1997 Oct 20;416(2):175-8. doi: 10.1016/s0014-5793(97)01197-6. PMID: 9369208.

15. Damle VG, Sharmin R, Morita A, Nie L, Schirhagl R. Micro Versus Macro - The Effect of Environmental Confinement on Cellular Nanoparticle Uptake. Front Bioeng Biotechnol. 2020 Jul 24;8:869. doi: 10.3389/fbioe.2020.00869. PMID: 32793585; PMCID: PMC7393206.

16. Balasubramanian G, Chan IY, Kolesov R, Al-Hmoud M, Tisler J, Shin C, Kim C, Wojcik A, Hemmer PR, Krueger A, Hanke T, Leitenstorfer A, Bratschitsch R, Jelezko F, Wrachtrup J. Nanoscale imaging magnetometry with diamond spins under ambient conditions. Nature. 2008 Oct 2;455(7213):648-51. doi: 10.1038/nature07278. PMID: 18833276.

17. Dolde F, Fedder H, Doherty MW, Nöbauer T, Rempp F, Balasubramanian G, Wolf T, Reinhard F, Hollenberg LCL, Jelezko F, Wrachtrup J. Electric-field sensing using single diamond spins. Nat. Phys. 2011; 7: 459–463. doi:10.1038/NPHYS1969.

18. Kucsko G, Maurer PC, Yao NY, Kubo M, Noh HJ, Lo PK, Park H, Lukin MD. Nanometre-scale thermometry in a living cell. Nature. 2013 Aug 1;500(7460):54-8. doi: 10.1038/nature12373. PMID: 23903748; PMCID: PMC4221854.

19. Neumann P, Jakobi I, Dolde F, Burk C, Reuter R, Waldherr G, Honert J, Wolf T, Brunner A, Shim JH. High-precision nanoscale temperature sensing using single defects in diamond. Nano Lett. 2013 Jun 12;13(6):2738-42. doi: 10.1021/nl401216y. PMID: 23721106.

20. Toyli DM, de las Casas CF, Christle DJ, Dobrovitski VV, Awschalom DD. Fluorescence thermometry enhanced by the quantum coherence of single spins in diamond. Proc Natl Acad Sci U S A. 2013 May 21;110(21):8417-21. doi: 10.1073/pnas.1306825110. Epub 2013 May 6. PMID: 23650364; PMCID: PMC3666694.

21. Momenzadeh A, de Oliveira FF, Neumann P, Rao B, Denisenko A, Amjadi M, Chu Z, Yang S, Manson NB, Doherty MW, Wrachtrup J. Thin circular diamond membrane with embeddenitrogen-vacancy centers for hybrid spin-mechanical quantum systems. PhysRev. Applied. 2016; 6(2): 024026. doi:10.1103/PhysRevApplied.6.024026.

22. Grinolds MS, Hong S, Maletinsky P, Luan L, Lukin MD, Walsworth RL, Yacoby A. Nanoscale magnetic imaging of a single electron spin under ambient conditions. Nat. Phys. 2013; 9: 215–219. doi:10.1038/NPHYS2543.

23. Sharmin R, Hamoh T, Sigaeva A, Mzyk A, Damle VG, Morita A, Vedelaar T, Schirhagl R. Fluorescent Nanodiamonds for Detecting Free-Radical Generation in Real Time during Shear Stress in Human Umbilical Vein Endothelial Cells. *ACS Sensors. 2021; 6*(12): 4349-4359. https://doi.org/10.1021/acssensors.1c01582

24. Nie L, Nusantara AC, Damle VG, Sharmin R, Evans EPP, Hemelaar SR, van der Laan KJ, Li R, Perona Martinez FP, Vedelaar T, Chipaux M, Schirhagl R. Quantum monitoring of cellular metabolic activities in single mitochondria. Sci Adv. 2021 May 19;7(21):eabf0573. doi: 10.1126/sciadv.abf0573. PMID: 34138746; PMCID: PMC8133708.

25. Tetienne J, Hingant T, Rondin L, Cavaillès A, Mayer L, Dantelle G, Gacoin T, Wrachtrup J, Roch J, Jacques V . Spin relaxometry of single nitrogen-vacancy defects in diamond nanocrystals for magnetic noise sensing. Phy RevB 2013; 87: 235436. doi:10.1103/physRevB.87.235436.

26. Hemelaar SR, Nagl A, Bigot F, Rodríguez-García MM, de Vries MP, Chipaux M, Schirhagl R. The interaction of fluorescent nanodiamond probes with cellular media. Microchim. Acta. 2017;184(4):1001-1009. doi: 10.1007/s00604-017-2086-6. Epub 2017 Jan 27. PMID: 28344361; PMCID: PMC5346409.

27. Morita A, Martinez F PP, Chipaux M, Jamot N, Hemelaar SR, van der Laan KJ, Schirhagl R. Cell uptake of lipid-coated diamond. Particle and Particle Systems Characterization 2019; 36: 1900116. doi.org/10.1002/ppsc.201900116.

28. Shenderova OA, Shames AI, Nunn NA, Torelli MD, Vlasov I, Zaitsev A. Review Article: Synthesis, properties, and applications of fluorescent diamond particles. J Vac Sci Technol B Nanotechnol Microelectron. 2019 May;37(3):030802. doi: 10.1116/1.5089898. Epub 2019 Apr 12. PMID: 31032146; PMCID: PMC6461556.

29. Hemelaar SR, de Boer P, Chipaux M, Zuidema W, Hamoh T, Martinez FP, Nagl A, Hoogenboom JP, Giepmans BNG, Schirhagl R. Nanodiamonds as multi-purpose labels for microscopy. Sci Rep. 2017 Apr 7;7(1):720. doi: 10.1038/s41598-017-00797-2. PMID: 28389652; PMCID: PMC5429637.

30. Schindelin J, Arganda-Carreras I, Frise E, Kaynig V, Longair M, Pietzsch T, Preibisch S, Rueden C, Saalfeld S, Schmid B, Tinevez JY, White DJ, Hartenstein V, Eliceiri K, Tomancak P, Cardona A. Fiji: an open-source platform for biological-image analysis. Nat Methods. 2012 Jun 28;9(7):676-82. doi: 10.1038/nmeth.2019. PMID: 22743772; PMCID: PMC3855844.

31. Bolte S, Cordelières FP. A guided tour into subcellular colocalization analysis in light microscopy. J Microsc. 2006 Dec;224(Pt 3):213-32. doi: 10.1111/j.1365-2818.2006.01706.x. PMID: 17210054.

32. Dunn KW, Kamocka MM, McDonald JH. A practical guide to evaluating colocalization in biological microscopy. Am J Physiol Cell Physiol. 2011 Apr;300(4):C723-42. doi: 10.1152/ajpcell.00462.2010. Epub 2011 Jan 5. PMID: 21209361; PMCID: PMC3074624.

33. Manders EMM, Verbeek FJ, Aten JA. Measurement of co-localization of objects in dual-colour confocal images. J Microsc. 1993 Mar;169(3):375-382. doi: 10.1111/j.1365-2818.1993.tb03313.x. PMID: 33930978.

34. Morita A, Hamoh T, Martinez FPP, Chipaux M, Sigaeva A, Mignon C, Laan KJV, Hochstetter A, Schirhagl R. The Fate of Lipid-Coated and Uncoated Fluorescent Nanodiamonds during Cell Division in Yeast. Nanomaterials (Basel). 2020 Mar 12;10(3):516. doi: 10.3390/nano10030516. PMID: 32178407; PMCID: PMC7153471.

35. Perona Martínez F, Nusantara AC, Chipaux M, Padamati SK, Schirhagl R. Nanodiamond Relaxometry-Based Detection of Free-Radical Species When Produced in Chemical Reactions in Biologically Relevant Conditions. ACS Sens. 2020 Dec 24;5(12):3862-3869. doi: 10.1021/acssensors.0c01037. Epub 2020 Dec 3. PMID: 33269596; PMCID: PMC8651177.

36. Jones CI 3rd, Han Z, Presley T, et al. Endothelial cell respiration is affected by the oxygen tension during shear exposure: role of mitochondrial peroxynitrite. American Journal of physiology. Cell Physiology. 2008 Jul;295(1):C180-91. DOI: 10.1152/ajpcell.00549.2007. PMID: 18480296; PMCID: PMC2493556.

37. Hemelaar SR, Saspaanithy B, L'Hommelet SRM, Perona Martinez FP, van der Laan KJ, Schirhagl R. The Response of HeLa Cells to Fluorescent NanoDiamond Uptake. Sensors (Basel). 2018 Jan 26;18(2):355. doi: 10.3390/s18020355. PMID: 29373504; PMCID: PMC5855215.

38. Chu Z, Zhang S, Zhang B, Zhang C, Fang CY, Rehor I, Cigler P, Chang HC, Lin G, Liu R, Li Q. Unambiguous observation of shape effects on cellular fate of nanoparticles. Sci Rep. 2014 Mar 28;4:4495. doi: 10.1038/srep04495. PMID: 24675513; PMCID: PMC3968459.

39. Chu Z, Miu K, Lung P, Zhang S, Zhao S, Chang HC, Lin G, Li Q. Rapid endosomal escape of prickly nanodiamonds: implications for gene delivery. Sci Rep. 2015 Jun 30;5:11661. doi: 10.1038/srep11661. PMID: 26123532; PMCID: PMC4485068.

40. Zhang Y, Sharmin R, Sigaeva A, Klijn CWM, Mzyk A, Schirhagl R. Not all cells are created equal - endosomal escape in fluorescent nanodiamonds in different cells. Nanoscale. 2021 Aug 21;13(31):13294-13300. doi: 10.1039/d1nr02503a. Epub 2021 Jul 20. PMID: 34477735.

41. Van der Laan KJ, Naulleau J, Damle VG, Sigaeva A, Jamot N, Perona-Martinez FP, Chipaux M, Schirhagl R. Toward Using Fluorescent Nanodiamonds To Study Chronological Aging in Saccharomyces cerevisiae. Anal Chem. 2018 Nov 20;90(22):13506-13513. doi: 10.1021/acs.analchem.8b03431. Epub 2018 Oct 31. PMID: 30345733.

42. Nie L, Nusantara AC, Damle VG, Baranov MV, Chipaux M, Reyes-San-Martin C, Hamoh T, Epperla CP, Guricova M, Cigler P, van den Bogaart G, Schirhagl R. Quantum Sensing of Free Radicals in Primary Human Dendritic Cells. Nano Lett. 2022 Feb 23;22(4):1818-1825. doi: 10.1021/acs.nanolett.1c03021. Epub 2021 Dec 20. PMID: 34929080; PMCID: PMC8880378.

43. Thekra Al-Belooshi, Annie John, Saeed Tariq, Amna Al-Otaiba, Haider Raza. Increased mitochondrial stress and modulation of mitochondrial respiratory enzyme activities in acetaminophen-induced toxicity in mouse macrophage cells. Food Chem Toxicol. 2010 Oct;48(10):2624-32. doi: 10.1016/j.fct.2010.06.031. Epub 2010 Jun 22. PMID: 20600533.

44. Hongslo JK, Bjørnstad C, Schwarze PE, Holme JA. Inhibition of replicative DNA synthesis by paracetamol in V79 Chinese hamster cells. Toxicol In Vitro. 1989;3(1):13-20. doi: 10.1016/0887-2333(89)90018-0. PMID: 20702318.

45. Rannug U, Holme JA, Hongslo JK, Srám R. International Commission for Protection against Environmental Mutagens and Carcinogens. An evaluation of the genetic toxicity of paracetamol. Mutat Res. 1995 Mar;327(1-2):179-200. doi: 10.1016/0027-5107(94)00184-7. PMID: 7870087.

46. Greenley TL, Davies MJ. Direct detection of radical generation in rat liver nuclei on treatment with tumour-promoting hydroperoxides and related compounds. Biochim Biophys Acta. 1994 Apr 12;1226(1):56-64. doi: 10.1016/0925-4439(94)90059-0. PMID: 8155740.

47. Van der Laan K, Hasani M, Zheng T, Schirhagl R. Nanodiamonds for In Vivo Applications. Small. 2018 May;14(19):e1703838. doi: 10.1002/smll.201703838. Epub 2018 Feb 9. PMID: 29424097.

48. Kaja S, Payne AJ, Naumchuk Y, Levy D, Zaidi DH, Altman AM, Nawazish S, Ghuman JK, Gerdes BC, Moore MA, Koulen P. Plate reader-based cell viability assays for glioprotection using primary rat optic nerve head astrocytes. Exp Eye Res. 2015 Sep;138:159-66. doi: 10.1016/j.exer.2015.05.023. Epub 2015 Jun 3. PMID: 26048476; PMCID: PMC4553084.

49. Eruslanov E, Kusmartsev S. Identification of ROS using oxidized DCFDA and flow-cytometry. Methods Mol Biol. 2010;594:57-72. doi: 10.1007/978-1-60761-411-1_4. PMID: 20072909.

50. Lindberg E, Winssinger N. High Spatial Resolution Imaging of Endogenous Hydrogen Peroxide in Living Cells by Solid-State Fluorescence. Chembiochem : a European Journal of Chemical Biology. 2016 Sep;17(17):1612-1615. DOI: 10.1002/cbic.201600211. PMID: 27271247.

51. Li N, Ragheb K, Lawler G, Sturgis J, Rajwa B, Melendez JA, Robinson JP. Mitochondrial complex I inhibitor rotenone induces apoptosis through enhancing mitochondrial reactive oxygen species production. J Biol Chem. 2003 Mar 7;278(10):8516-25. doi: 10.1074/jbc.M210432200. Epub 2002 Dec 20. PMID: 12496265.

52. Bucana C, Saiki I, Nayar R. Uptake and accumulation of the vital dye hydroethidine in neoplastic cells. J Histochem Cytochem. 1986 Sep;34(9):1109-15. doi: 10.1177/34.9.2426339. PMID: 2426339.

Supplementary

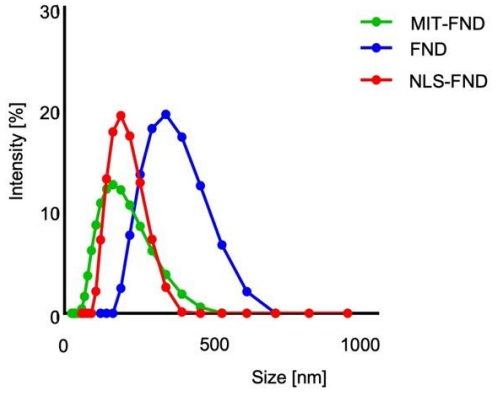

Supplementary Figure S1: Size distributions of FND, NLS-FNDs and MIT-FND in DMEM medium. FNDs have an average size of 342 nm, while MIT-FNDs and NLS-FNDs average sizes are 290 and 190nm in DMEM medium. All measurements were performed three independent times at 37° C. The reason for the reduced size of the conjugated particles is that an existing protein layer on the particles prevents aggregation as shown in [26].

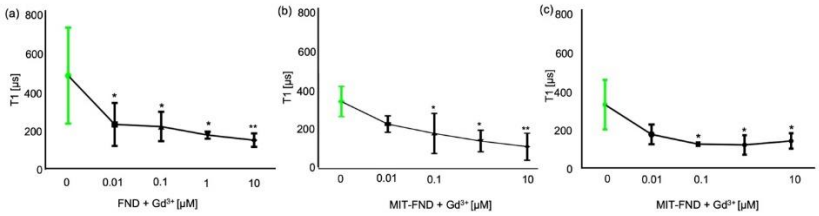

Supplementary Figure S2: Evaluation of spin sensing capacity of FNDs, MIT-FNDs and NLS-FNDs with differently concentrated $GdCl_3$. $GdCl_3$solutions were added to DMEM high glucose medium for measuring T1. The error bars represent the standard error of the mean from 4 particles. The data were analyzed using a one-way ANOVA followed by a Tukey post hoc test. Statistical significance is indicated by *P $\leq$0.05, **P $\leq$ 0.01.

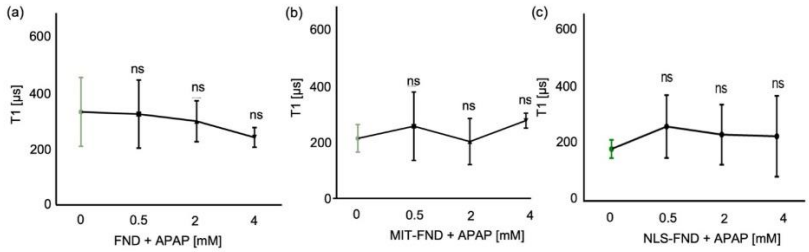

Supplementary Figure S3: Control experiments: FNDs, MIT-FNDs and NLS-FNDs without cells were exposed to APAP. T1 values were measured only in DMEM glucose medium by adding different concentrations of APAP. The error bars represent the standard error mean from 4 particles. Ns means non significant. The data were analyzed using a one-way ANOVA followed by a Tukey post hoc test. Statistical significance is indicated by ns > 0.05

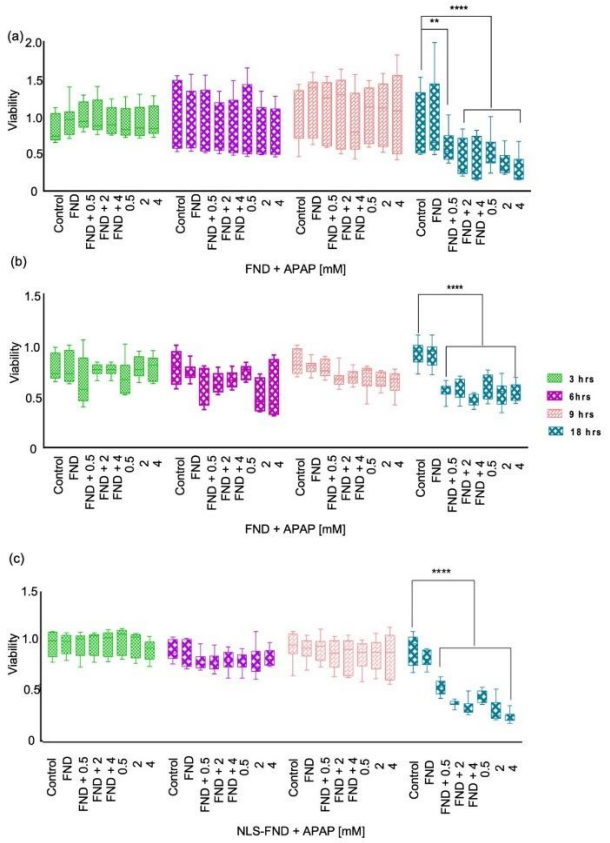

Supplementary Figure S4: cell viability after exposure of cells with FNDs, MIT-FNDs and NLS-FNDs in the presence of different concentrations of APAP. Cell viabilities were compared with the corresponding control groups. The data is shown by separated box and whisker plots with minimum and maximum values. Each experiment was repeated 3 independent times. Data were analyzed using two-way ANOVA followed by a Tukey post hoc test. Statistical significance is indicated by *P ≤0.05, **P ≤ 0.01, ****P≤0.0001

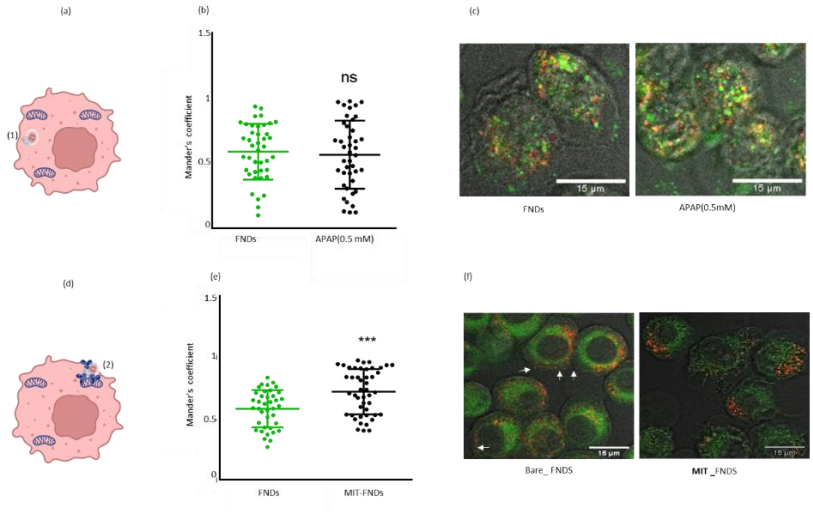

Supplementary Figure S5: Confirming the location of particles, (b) Colocalization of FNDS with vesicles (stained with calcein) determined by Manders' colocalization coefficient. As shown before [26] FNDs escape from endosomes and thus do not colocalize with calcein. We also show that the location does not change in the groups treated with APAP (0.5mM) for 18h. (c) Confocal images showing the FNDs (red) escaped from endosomes (vesicles stained in green). (e) shows the colocalization of MIT-FNDs and FNDs with mitochondria analyzed by using the Mander's colocalization coefficient. (f) Representative confocal images showing FND and MIT-FNDs (red) and mitochondria (green) stained with Mito Tracker green that specifically stains mitochondria. Scatter dot plots show the standard deviations. The scatter dot plots show the standard deviations (unpaired t-test, ***$p \leq 0.001$). Experiments were repeated 3 independent times.

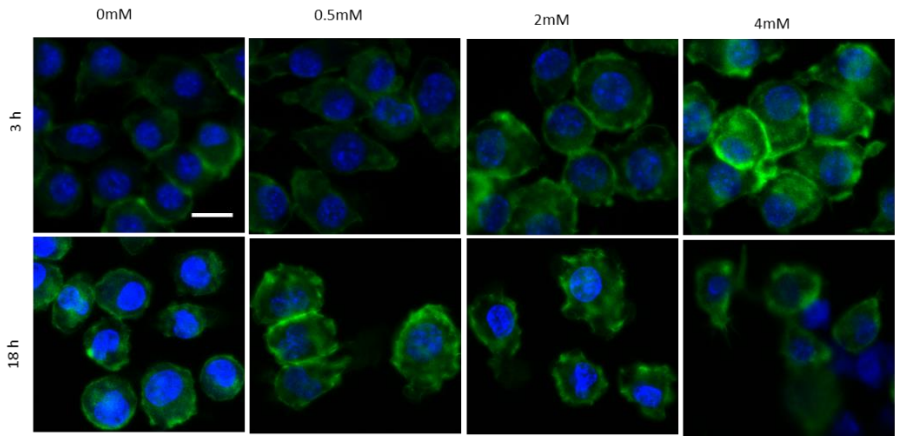

Supplementary Figure S6: Confocal images show the confluency loss after 18 h of APAP treatment compared to 3 h of APAP treatment. Most of the cells from the 18 h treatment groups were washed out during the following steps of staining whereas cells from 3 h APAP treatment groups were retained and maintained the confluency. Scale bar is 15 µm.